arXiv:astro-ph/0301530v1 27 Jan 2003

Large Scale Alignment of Optical Polarizations from Distant QSOs using Coordinate Invariant Statistics

Pankaj Jain, Gaurav Narain and S. Sarala
Physics Department, I.I.T. Kanpur, India 208016
email : pkjain@iitk.ac.in

February 2, 2008

Abstract

We introduce several coordinate invariant statistical procedures in order to test for local alignment of polarizations. A large scale alignment of optical polarizations from distant QSOs has recently been observed by Hutsemékers and collaborators. The new statistical procedures are based on comparing polarizations at different angular coordinates by making a parallel transport. The results of these statistical procedures continue to support the existence of the large scale alignment effect in the QSO optical polarization data. The alignment is found to be much more pronounced in the data sample with low degrees of polarization $p \leq 2\%$. This suggests that the alignment may be attributed to some propagation effect. The distance scale over which the alignment effect is dominant is found to be of order 1 Gpc. We also find that a very large scale alignment is present in the large redshift, $z \geq 1$, data sample. Infact the data sample with $z \geq 1$ appears to be aligned over the entire celestial sphere. We discuss possible physical effects, such as extinction and pseudoscalar-photon mixing, which may be responsible for the observations.

Key words : polarization: magnetic fields: elementary particles: methods - data analysis, statistical: quasars - general.

1 Introduction

The optical polarizations from QSOs appear to be aligned with one another over very large distances (Hutsemékers 1998). This effect was further confirmed by Hutsemékers & Lamy (2001) using a larger data set. It was observed that the polarizations from QSOs in any particular spatial region

or a patch have a tendency to align with one another, without any evidence of a large scale anisotropy. The effect was found to be redshift dependent, namely the patches which are aligned are delimited both in angular as well as radial (redshift) coordinates. A very striking alignment was found in the region, called A1 by Hutsemékers (1998), delimited in Right Ascension by $11^{\rm h}15^{\rm m} \leq {\rm RA} \leq 14^{\rm h}29^{\rm m}$ and in redshift by $1.0 \leq z \leq 2.3$. By using several statistical tests (Hutsemékers 1998; Hutsemékers & Lamy 2001) the authors were able to rule out the hypothesis of uniform distribution at approximately 0.1% significance level. The basic idea behind these statistical procedures is to test for the dispersion in the orientations of polarizations in any small neighbourhood. The tests require comparing the polarization vectors located at different angular coordinates. These polarizations are specified by the angles they make with respect to the local meridians (Hutsemékers 1998). The statistical tests used by Hutsemékers (1998) are, however, dependent on the precise position of the pole used for defining the coordinate system and hence it is difficult to interpret the results obtained by these tests. In the present paper we introduce some statistical tests which are independent of the coordinate system and apply them to the QSO optical polarization data.

2 Parallel Transport

The basic problem can be explained as follows. Consider two tangent vectors $\boldsymbol{v_1}$ and $\boldsymbol{v_2}$ located at two different points $\rm P_1$ and $\rm P_2$ on the surface of the sphere. These vectors are specified at each point on the sphere in terms of the angle they make with respect to the local unit vector $\hat{\phi}$. Here we have chosen the spherical polar coordinate system defined by the unit vectors $(\hat{r}, \hat{\theta}, \hat{\phi})$. Let α_1 be the angle made by the vector $\boldsymbol{v_1}$ with respect to the local unit vector $\hat{\phi}_1$ at the location $\rm P_1$. Similarly let α_2 be the angle made by the vector $\boldsymbol{v_2}$ with respect to the local unit vector $\hat{\phi}_2$ at the location $\rm P_2$. The two vectors in their local coordinates are given by

$$\boldsymbol{v_1} = \cos\alpha_1\hat{\phi}_1 + \sin\alpha_1\hat{\theta}_1$$
$$\boldsymbol{v_2} = \cos\alpha_2\hat{\phi}_2 + \sin\alpha_2\hat{\theta}_2$$

In order to compare these two vectors we may use the usual dot product,

$$\boldsymbol{v_1} \cdot \boldsymbol{v_2} = \cos(\alpha_1)\cos(\alpha_2) + \sin(\alpha_1)\sin(\alpha_2)\ . \qquad (1)$$

However this dot product is not invariant under coordinate transformation and hence a statistical procedure based on this will be coordinate dependent.

A coordinate invariant dot product may be obtained if we parallel transport $\boldsymbol{v_1}$ to P_2 and then take the dot product of the transported vector $\boldsymbol{v_1}'$ with $\boldsymbol{v_2}$. Let the parallel transported vector $\boldsymbol{v_1}'$ make the angle α_1' with respect to $\hat{\phi}_2$. We are interested in finding α_1' which can then allow us to calculate the angle $\alpha_1' - \alpha_2$ between the parallel transported vector $\boldsymbol{v_1}'$ and the vector $\boldsymbol{v_2}$.

Let $\hat{r}_1$ and $\hat{r}_2$ be unit radial vectors at the points P_1 and P_2 respectively. The unit vector $\hat{s}$ perpendicular to the plane containing these two radial vectors is given by

$$\hat{s} = \frac{\hat{r}_1 \times \hat{r}_2}{|\hat{r}_1 \times \hat{r}_2|} \tag{2}$$

Therefore the unit tangent vectors $\hat{t}_1$ and $\hat{t}_2$ at the two points P_1 and P_2 respectively along the great circle passing through these two points are given by,

$$\hat{t}_1 = \hat{s} \times \hat{r}_1 \tag{3}$$

$$\hat{t}_2 = \hat{s} \times \hat{r}_2 \tag{4}$$

In terms of the local basis $(\hat{\theta}, \hat{\phi})$ these two vectors are given by

$$\hat{t}_1 = \hat{\theta}_1 \cdot \hat{t}_1 \hat{\theta}_1 + \hat{\phi}_1 \cdot \hat{t}_1 \hat{\phi}_1 \tag{5}$$

$$\hat{t}_2 = \hat{\theta}_2 \cdot \hat{t}_2 \hat{\theta}_2 + \hat{\phi}_2 \cdot \hat{t}_2 \hat{\phi}_2 \tag{6}$$

where

$$\hat{\theta}_1 \cdot \hat{t}_1 = \frac{-\sin\theta_1 \cos\theta_2 + \cos\theta_1 \sin\theta_2 \cos(\phi_2 - \phi_1)}{\sqrt{1 - (\hat{r}_1 \cdot \hat{r}_2)^2}} \tag{7}$$

$$\hat{\phi}_1 \cdot \hat{t}_1 = \frac{\sin\theta_2 \sin(\phi_2 - \phi_1)}{\sqrt{1 - (\hat{r}_1 \cdot \hat{r}_2)^2}} \tag{8}$$

$$\hat{\theta}_2 \cdot \hat{t}_2 = -\frac{-\sin\theta_2 \cos\theta_1 + \cos\theta_2 \sin\theta_1 \cos(\phi_2 - \phi_1)}{\sqrt{1 - (\hat{r}_1 \cdot \hat{r}_2)^2}} \tag{9}$$

$$\hat{\phi}_2 \cdot \hat{t}_2 = \frac{-\sin\theta_1 \sin(\phi_1 - \phi_2)}{\sqrt{1 - (\hat{r}_1 \cdot \hat{r}_2)^2}} \tag{10}$$

As we parallel transport a vector along the great circle its angle with respect to the tangent to the great circle remains fixed. Hence in order to determine the angle by which the vector has turned due to parallel transport we only need to find the orientation of $\hat{t}_1$ and $\hat{t}_2$ with respect to the local basis at the points P_1 and P_2 respectively. The angle ξ_1 between $\hat{t}_1$ and $\hat{\phi}_1$ is given by $\cos^{-1}(\hat{\phi}_1 \cdot \hat{t}_1)$. This gives ξ_1 upto an overall addition of π, which is fixed by the sign of $\hat{\theta}_1 \cdot \hat{t}_1$. If $\hat{\theta}_1 \cdot \hat{t}_1 < 0$ then ξ_1 lies in the third or

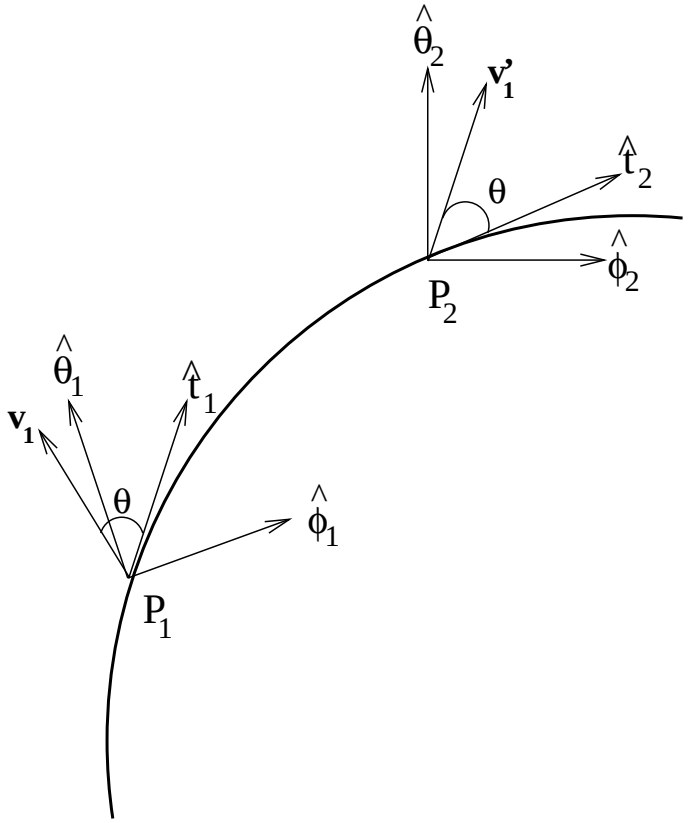

Figure 1: The curve is the great circle passing through points P_1 and P_2. t_1 and t_2 are the tangent vectors at points P_1 and P_2 respectively. Polarization vector v_1 from location P_1 is parallel transported to location P_2. Parallel transported vector is indicated by v_1'.

fourth quadrand. The angle ξ_2 is obtained in a similar manner. Hence the transported vector $\boldsymbol{v_1}'$ makes an angle $(\alpha_1 + \xi_2 - \xi_1)$ with respect to the $\hat{\phi}_2$. Therefore the rule for comparing vectors at two different locations on the sphere is given by the generalized dot product,

$$\boldsymbol{v_1} \odot \boldsymbol{v_2} = |\boldsymbol{v_1}||\boldsymbol{v_2}| \cos(\alpha_1 - \alpha_2 + \xi_2 - \xi_1) \ , \tag{11}$$

i.e. the dotproduct between the parallel transported vector $\boldsymbol{v_1}'$ and the vector $\boldsymbol{v_2}$.

In our discussion so far we have explained the procedure for comparing the vectors at two different points. The polarization orientations α_1 and α_2 at two different points P_1 and P_2 respectively can also be compared in a similar manner. We associate the unit vectors $\boldsymbol{v_1} = [\cos(2\alpha_1), \sin(2\alpha_1)]$ and $\boldsymbol{v_2} = [\cos(2\alpha_2), \sin(2\alpha_2)]$ with the polarizations at P_1 and P_2 respectively. We parallel transport the polarization α_1 to the location P_2. The angle between the parallel transported polarization and the unit vector $\hat{\phi}_2$ along the local ϕ axis at P_2 is equal to $\alpha_1' = (\alpha_1 + \xi_2 - \xi_1)$. We can assign a unit vector $\boldsymbol{v_1'} = [\cos(2\alpha_1'), \sin(2\alpha_1')]$ with this transported polarization. We then define the generalized product (α_1, α_2) between the two polarizations as the ordinary dot product between the two vector $\boldsymbol{v_1'}$ and $\boldsymbol{v_2}$

$$(\alpha_1, \alpha_2) = \boldsymbol{v_1'} \cdot \boldsymbol{v_2} = \cos[2(\alpha_1 - \alpha_2 + \xi_2 - \xi_1)] \ . \tag{12}$$

3 Statistical Tests for Alignment

The simplest statistics to test the alignment of vectors is to calculate the dispersion of the polarization with respect to its nearest neighbours. Consider the n_v nearest neighbours of the vector $\boldsymbol{v_i} = [\cos(2\theta_i), \sin(2\theta_i)]$ located at the i-th location, including the vector $\boldsymbol{v_i}$ itself. Here θ_i is the polarization orientation. The orientation angle may be measured with respect to the local meridian or the local latitude. Our final results depend only on the differences of angles and hence our formulae are directly applicable for either definition. The nearest neighbours are determined by computing the relative distance in three dimensions with the co-moving radial distance $r(z)$ given in terms of the redshift z by the standard relation,

$$r(z) = \frac{2c}{H_0} \left[1 - (1+z)^{-1/2}\right] \tag{13}$$

where H_0 is the Hubble constant and c is the velocity of light. A measure of the dispersion d_i of these set of vectors is given by,

$$\begin{aligned} d_i(\theta) &= \sum_{k=1}^{n_v} (\theta, \theta_k) \\ &= \sum_{k=1}^{n_v} \cos\left[2\theta - 2\left(\theta_k + \Delta_{k\to i}\right)\right] \end{aligned} \tag{14}$$

where $\Delta_{k\to i}$ is the angle by which the polarization orientation angle θ_k changes after being parallel transported to the position of the polarization angle θ_i and θ is a measure of the mean polarization at the i-th position. The symbol (θ, θ_k) is defined in Eq. 12. Hence d_i is calculated by parallel transporting the n_v nearest neighbours of the polarization θ_i to the i-th position and then taking the dot product of the resulting n_v vectors $\boldsymbol{v'_k} = [\cos(2\theta_k + 2\Delta_{k\to i})]$ with the vector $\boldsymbol{v}(\theta) = [\cos(2\theta), \sin(2\theta)]$. The n_v nearest neighbours include the vector $\boldsymbol{v_i}$ itself. The magnitude of $d_i(\theta)$ is then maximized with respect to θ. The resulting vector $\boldsymbol{v}(\theta)$ gives a measure of the local mean direction and the magnitude of the maximized $d_i(\theta)$ gives the measure of dispersion. We define the statistic as follows,

$$S_D^p = \frac{1}{n} \sum_{i=1}^{n} d_i|_{\max} \tag{15}$$

where the sum is over the entire data sample. A large value of d_i implies small dispersion and hence a large S_D^p would imply a strong alignment between the polarization vectors.

It is clear that the mean value $\overline{S_D^p}$ of this statistic for a random sample is proportional to $1/\sqrt{n_v}$. We verify this explicitly by numerical simulations. For $n_v = 25$ we find that the mean value $\overline{S_D^p} = 0.178$. In Fig. 2 we show the histogram of the statistic S_D^p obtained by using 10000 random samples with $n_v = 25$. The distribution tends to a normal distribution for large data samples. The distribution for different values of n_v was found to be identical except for a shift in the mean position, which as mentioned above, varies as $1/\sqrt{n_v}$. In our calculations we evaluated the statistical significance level (S. L.) for each case by explicit numerical simulation using a large number of random samples. The S. L. is defined as the probability that the value of the statistic obtained from the data may be obtained as a statistical fluctuation from a random sample. It is numerically evaluated by computing the statistic $(S*)$ of the data sample with the statistic S obtained from a large number of random samples. The S. L. is a probability that $S < S*$.

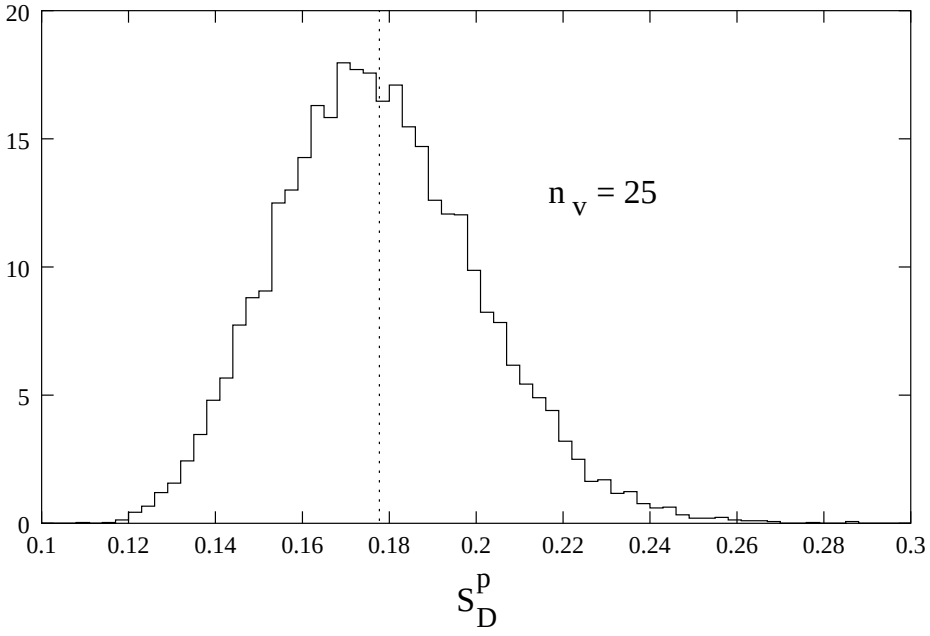

Figure 2: The histogram of the statistic S_D^p using 10000 random sample with the number of nearest neighbours $n_v = 25$. The mean position of the statistic for a random sample is shown by the verticle line.

Our second statistical test is the modified Andrews & Wasserman test, which was used by Hutsemékers (1998) and Hutsemékers & Lamy (2001). We first review this test. For each vector $\boldsymbol{v_j} = (\cos 2\theta_j, \sin 2\theta_j)$ the mean resultant vector with respect to its n_v nearest neighbours can be written as

$$\boldsymbol{V_j} = \frac{\mathcal{N}}{n_v}\left(\sum_{k=1}^{n_v}\cos 2\theta_k, \sum_{k=1}^{n_v}\sin 2\theta_k\right) \ . \tag{16}$$

where $\mathcal{N}$ is a normalization constant such that the vector V_j is normalized to unity. The sum over the nearest neighbours n_v excludes the j-th vector itself. We then define the mean direction $\bar{\theta_j}$ such that $\boldsymbol{V_j} = (\cos 2\bar{\theta_j}, \sin 2\bar{\theta_j})$. A measure of the alignment of vector $\boldsymbol{v_i} = (\cos 2\theta_i, \sin 2\theta_i)$ with the n_v nearest neighbours of the vector $\boldsymbol{v_j} = (\cos 2\theta_j, \sin 2\theta_j)$ is given by the dot product $D_{ij} = \boldsymbol{v_i} \cdot \boldsymbol{V_j}$. In order to evaluate the statistic, the D_{ij}, $j = 1, .., n$, values are sorted in the ascending order for each i. The rank $\mathcal{R}_i$ of $D_{i,j=i}$ is then evaluated. If n is the number of sources in the sample then the statistic is given as

$$Z_c = \frac{1}{n_v}\sum_{i=1}^{n}\frac{\mathcal{R}_i - (n+1)/2}{\sqrt{n/12}} \tag{17}$$

As shown by Bietenholz (1986), the statistic Z_c approximately follows a normal distribution. However we did not use this asymptotic result in obtaining our S. L. but evaluated it explicitly by using a large number of random samples. The Andrews and Wasserman test can be modified (Hutsemékers 1998) by using the unnormalized vector V_j, i.e. by setting the normalization constant $\mathcal{N}$ to unity. The resulting statistic is denoted by Z_c^m (Hutsemékers 1998).

As explained earlier this statistic is not coordinate invariant since it compares the vectors at different locations without making a parallel transport. We can modify this statistic by using the generalized product, Eq. 12, to compare polarizations at different positions. We therefore express D_{ij} directly in terms of the coordinate invariant quantity (θ_i, θ_k). The basic idea behind the calculation of D_{ij} is to compare i-th polarization θ_i with the n_v nearest neighbours θ_k of the j-th polarization θ_j. Hence one possible coordinate invariant definition of D_{ij} is

$$\begin{aligned} D_{ij}^p &= \frac{1}{n_v}\sum_{k=1}^{n_v}(\theta_i, \theta_k) \\ &= \frac{1}{n_v}\sum_{k=1}^{n_v}\cos\left[2\theta_i - 2\left(\theta_k + \Delta_{k\to i}\right)\right] \end{aligned} \tag{18}$$

where θ_k, $k = 1, ..., n_v$ are the n_v nearest neighbours of the polarization θ_j, excluding θ_j itself. Hence all the n_v polarizations are compared to the polarization θ_i after parallel transporting them to the i-th position. It is clear that if we replace the generalized product with the ordinary dot product in this equation, i.e. if we set $\Delta_{k\to i} = 0$, then D^p_{ij} reduces to the matrix D_{ij} that is used in the Andrews & Wasserman test with the normalization factor $\mathcal{N}$ in Eq. 16 set equal to unity. D^p_{ij} is the measure of alignment between the i-th vector and n_v nearest neighbours of the j-th vector. The statistic is then calculated in a manner similar to that used in the Andrews & Wasserman test. We again arrange D^p_{ij}, $j = 1, .., n$, in ascending order and obtain the rank $\mathcal{R}_i$ of $D^p_{i,j=i}$. The statistic is calculated using equation 17 and is called Z^p_c.

Another somewhat more complicated coordinate invariant definition of D_{ij} can be obtained by parallel transporting all the polarizations to the position of the polarization $\boldsymbol{v_j}$ and then comparing them at this point. The resulting expression is given by,

$$D^{p\prime}_{ij} = \frac{1}{n_v}\sum_{k=1}^{n_v} \cos\left\{[2\theta_j - 2\left(\theta_k + \Delta_{k\to j}\right)] - [2\theta_j - 2\left(\theta_i + \Delta_{i\to j}\right)]\right\} \qquad (19)$$

This can also be explicitly expressed in terms of the basic coordinate invariant quantity, (θ_i, θ_j), but the precise expression is not needed here. The results obtained by using $D^{p\prime}_{ij}$ are similar to those obtained by using D^p_{ij}.

3.1 Coordinate Invariance

We next test explicitly whether the statistics defined in the previous section are indeed invariant under coordinate transformations. Consider a polarization which is oriented at an angle θ and located at the position (α, δ) in a particular coordinate system. Next we consider a transformed coordinate frame such that its pole lies at the position (α_p, δ_p) in the original coordinates. Let the polarization be oriented at an angle θ_N in the new system. The angle θ_N can be expressed as (Hutsemékers 1998)

$$\tan\left(\theta - \theta_N\right) = \frac{\cos\delta_p \sin(\alpha_p - \alpha)}{\sin\delta_p\cos\delta - \sin\delta\cos\delta_p\cos(\alpha_p - \alpha)}\ . \qquad (20)$$

The angular position of the polarization can also be evaluated in the new coordinate system by making an orthogonal transformation. The coordinates are transformed by first making a rotation about x-axis by an angle $(-\delta_p + \pi/2)$ and then a rotation about the new z-axis by an angle $(-\alpha_p + \pi/2)$.

The resulting statistics S_D^p and Z_c^p for several choices of the pole position are given in Table 1, choosing the number of nearest neighbours $n_v = 20$. The coordinate independence of the statistic is clear from this table.

α_p	δ_p	S_D^p	Z_c^p
0	90	0.267563	2.069346
100	20	0.267581	2.069346
25	-80	0.267569	2.069346
150	55	0.267586	2.069346
30	-45	0.267568	2.069346

Table 1: The statistics S_D^p & Z_c^p for different choices of arbitrary poles (α_p, δ_p) with $n_v = 20$ nearest neighbours.

4 Results

The significance levels (S. L.) for the S_D^p and Z_c statistic are given in Figures 3-6. We plotted the logarithmic significance level of both the statistical tests Z_c^p and S_D^p as a function of n_v, the number of nearest neighbours. The S. L. was computed by numerical simulations which compares the data statistic with that of a large number N_S of random samples. For most cases the choice $N_S = 1000$ was found to be sufficient. In several cases it was found necessary to increase N_S to 10000 or larger in order to get a reasonable estimate of S.L.. In computing Z_c^p we used the matrix D_{ij}^p given in Eqn. (18). The matrix $D_{ij}^{p\prime}$, Eqn. (19), gave similar results. The results are obtained both by using the radial distance $r(z)$ given in Eqn. (13) as well as by setting $r(z) = 1$, which tests for a redshift independent alignment. We also try out several cuts based on the redshift z and the degree of polarization p. In Figs. 3,4 we show the significance level using the S_D^p statistic for redshift dependent and redshift independent alignment respectively. In Figs. 5,6 we show the signifigance level using the Z_c^p statistic for redshift dependent and redshift independent alignment respectively.

For an entire data set of 213 points we find that the $\log(S.L.) < -2.5$ over a wide range of n_v values using the S_D^p test for redshift dependent alignment. The minimum $\log(S.L.) = -2.92$ for $n_v = 32$. Hence we find that there is evidence for large scale alignment as observed by Hutsemékers (1998). The Z_c^p statistic (Fig. 5) also shows alignment with $log(S.L.) < -2$

for $n_v \geq 32$. The redshift independent test (Fig. 4 and 6) does not show any evidence of alignment for the complete sample. We also examined several cuts on the data sample in order to determine whether the alignment arises from large or small degrees of polarization and redshifts. We find that low polarizations $p \leq 2\%$ show a very significant redshift dependent alignment as seen in Figures 3 and 5. The number of data points with this cut is 146. The $\log(S.L.) = -4.0$ for $n_v = 24$ and 32 using the S_D^p statistic and reaches -5.0 for $n_v = 28$ with the Z_c^p statistic. The data with large polarization, $p \geq 1\%$, however, shows no evidence of alignment with any choice of the statistic. The number of data points in this case is 147. The fact that low polarizations are significantly aligned suggests that the effect may arise due to propagation.

We next compute the mean distance at which the alignment effect is most pronounced by directly testing for alignment over a certain distance, rather than using the number of nearest neighbours. In this case we test for alignment of a particular object with all the objects within a fixed distance of this object. Using the S_D^p statistic with $p \leq 2\%$ we find that the S.L. takes its minimum value at $r(z) \approx 0.22(2c/H_0)$, which corresponds to a distance scale of the order of a Gpc.

We next examine the cuts on redshifts. In Fig. 3 we find that the sources at large redshifts $z \geq 1$ show a very strong alignment with the S_D^p statistic for number of nearest neighbours larger than about 35. The number of objects in the data sample $z \geq 1$ are 115. For comparison we also consider a low redshift data sample, where the cut $z \leq 1.3$ is chosen such that it also contains approximately the same number of objects as the $z \geq 1$ sample. The $z \leq 1.3$ infact also contains 115 objects. From Figs. 3 and 4 we find that the large redshift sample shows a strong alignment independent of whether we take the radial distance of the object into account or set it equal to unity. Hence the alignment of objects at large redshifts is not necessarily redshift dependent. The low redshift objects, however, do not show a strong alignment with this statistic. The results for the Z_c^p statistic (Figs. 5 and 6), however, show no alignment for large redshift sources and a weak alignment for low redshifts. The fact that the S_D^p statistic shows a strong signal for alignment of large redshift objects and the Z_c^p shows no signal is easily understood. We find that the alignment of the large redshift sources occurs predominantly for relatively large number of nearest neighbours, and hence for large distances. The Z_c^p statistic dominantly tests only for local alignment. The S_D^p can test both local and large scale alignment. The large redshift points seem to be aligned over very large distances. This is shown more clearly in Fig. 7, which shows the $\log(S.L.)$

for very large values of n_v. The results for $p \leq 2\%$ cut are also shown for comparison. It is clear from this figure that the large redshift points show alignment over the entire sample. Hence we find that besides the redshift dependent alignment, which happens primarily for the objects with low polarization, the entire set of large redshift objects are aligned with one another. This effect is different from the redshift dependent alignment and was not noticed by Hutsemékers (1998). We emphasize that the redshift dependent alignment is seen dominantly for low polarizations as shown in fig. 3. The large redshift objects, however, show an alignment over the entire sky.

In order to understand this very large scale alignment at large redshifts, $z \geq 1$, we make a scatter plot of the objects which show a significant alignment along with those which do not. In this study we ignore the redshift dependence of the objects since the $z \geq 1$ set shows significant effect irrespective of whether we include or ignore the redshift dependence. From fig. 7 we find that the S.L. is minimum at $n_v = 38$ and hence we choose this value of n_v for our study. The resulting scatter plot is shown in fig. 8 where the pluses and dots refer to the objects for which the dispersion measure $d_i < 0.25$ and $d_i \geq 0.25$ respectively. We point out that the statistic $S_D^p = 0.307$ in this case. We choose $d_i = 0.25$ as the cutoff in this figure since it shows the boundary between the aligned and non-aligned sources clearly. A choice of $d_i = 0.3$ as the cutoff also leads to a similar scatter graph, but with a larger overlap between the aligned and non-aligned regions. Furthermore the figure does not change too much if we choose a larger value of n_v. It is clear from figure 8 that a large contribution to statistic is obtained from what is called the A1 region by Hutsemékers (1998). This region is centered roughly at the Virgo supercluster and is delimited in redshift such that $1 \leq z \leq 2.3$. However as can be seen from Fig. 8, other regions also show significant alignment.

In order to understand the nature of this very large scale alignment we first observe that the objects lying within the coordinate interval $10 \leq RA \leq 16$ and $-30 \leq Dec \leq 30$ are aligned with one another. Similarly the objects in the region $RA \geq 22$, $RA \leq 2$ and $-40 \leq Dec \leq 30$ are also aligned over this entire patch. Hence we find that the data splits into two large patches such that in each patch most of the objects show alignment with one another. The mean polarization angles, i.e. the mean over the $n_v = 38$ nearest neighbours, in the interval $10 \leq RA \leq 16$ are centered at the value of approximately 2.95 radians. In the region $RA \geq 22$, $RA \leq 2$, the means are centered around the value 2.35 radians. A parallel transport from $RA = 0$, $Dec = -5.0$ to $RA = 13$, $Dec = 0$ leads to a shift in the

polarization angle by 0.64 radians, which when added to 2.35 leads to an angle very close to 2.95. Hence we find that even these two widely separated regions are correlated. This explains the significant alignment observed in the entire data sample corresponding to $z \geq 1.0$ as shown in fig. 7.

5 Physical Explanation

The observation of such a large scale alignment is quite surprising and is not easily explained in terms of conventional astrophysics. QSOs at such large distances from one another are unlikely to be correlated with one another and hence the effect most likely arises due to propagation. The fact that the alignment is most dominant in the data sample with small polarizations further supports this hypothesis. Polarizations can show alignment with one another if they arise dominantly due to extinction. For example the galactic magnetic fields result in a large scale alignment of the dust particles, which preferentially attenuate a particular polarization component of the electromagnetic waves. Hence if the intrinsic source polarization is negligible, this will give rise to polarizations which are aligned over large distances. Galactic extinction, however, is unable to explain the redshift dependence of the effect. Furthermore it cannot explain why the large redshift points are correlated over such large distances, whereas the low redshift data shows no such correlation. We next examine the possibility that the alignment arises due to supercluster extinction. We assume that the magnitude of the supercluster extinction is large enough to cause such an alignment. The redshift dependent alignment seen in the low polarization sample ($p \leq 2\%$) can then be explained if we assume the presence of a few very large superclusters of distance scale of order 1 Gpc. The cosmological scale alignment seen in the large redshift sample is, however, not easily explained by this mechanism since we do not expect the presence of a supercluster which covers almost the entire celestial sphere at redshift of 1. Hence the observations are not completely explained in terms of galactic or supergalactic extinction.

Another physical phenomenon that can potentially explain the observations is the pseudoscalar-photon mixing (Hutsemékers & Lamy 2001; Jain, Panda & Sarala 2002). A light pseudoscalar particle is predicted by many extensions of the standard model of particle physics (for e.g. see Peccei & Quinn 1977; Mann & Moffat 1981; Sachs 1982; Will 1989; Ahluwalia & Goldman 1993; Ralston 1995). Its mixing with photons and its astrophysical consequences have also been studied by several authors (for e.g. see Sikivie 1983; Maiani, Petronzio & Zavattini 1986; Harari & Sikivie 1992; Das, Jain

& Mukherjee 2001). Its coupling to photons is bounded by observations of SN87A to be $g < 10^{-11}$ GeV^{-1} (Brockway, Carlson & Raffelt 1996; Grifols, Masso & Toldra 1996; Raffelt 1999; Rosenberg & van Bibber 2000). Such a particle has also be invoked to explain the observed dimming of supernovae at large redshifts even if the expansion rate of the universe is not accelerating (Csaki, Kaloper & Terning 2002). The pseudoscalar particle decays into photons in the presence of background magnetic field $\vec{B}$, such that the photon produced is polarized parallel to the transverse component of $\vec{B}$, which we denote as $\vec{B}_T$. Hence the electromagnetic wave produced by this mechanism is polarized parallel to $\vec{B}_T$. Similarly a photon polarized parallel to $\vec{B}$ can decay into the pseudoscalar during propagation, which leads to a wave polarized perpendicular to $\vec{B}_T$.

The existence of a hypothetical pseudoscalar can explain the observed alignment as follows. We first assume that the redshift dependent effect seen in low polarization objects is explained by the presence of a few superclusters of length scales of order 1 Gpc. As the electromagnetic waves pass through these superclusters the polarizations get aligned either due to extinction or due to pseudoscalar-photon mixing. We further assume that the large redshift objects, which show alignment over the entire sky, emit a large flux of the pseudoscalar particles whereas the flux emitted by low redshift objects is relatively small. This is reasonable since the large redshift objects are in general very active and have high temperatures. As these QSOs evolve they are less active and the pseudoscalar flux becomes negligible, which explains why the low redshift objects behave differently. As the pseudoscalars propagate through our local supercluster they decay into photons which are polarized parallel to the supercluster magnetic field. As discussed by Jain et al. (2002) the decay probability of such a pseudoscalar is of order unity with the current limits on the pseudoscalar-photon coupling. In obtaining this estimate we took the Virgo supercluster parameters for the magnetic field ($B \approx 1\mu G$) (Vallee 1990) and plasma density ($n_e \approx 10^{-6}$ cm^{-3}). We propose that a weaker magnetic field, $B \approx 0.1\mu G$, might be associated with the entire supercluster, and may be responsible for the observed alignment of large redshift objects over very large angular separations. We point out that the decay probability of pseudoscalars ϕ into photons γ, $P_{\phi\rightarrow\gamma} \sim B^2/n_e^2$ (Carlson & Garretson 1994; Jain et al. 2002) and hence even if the magnetic field is an order of magnitude smaller than that observed in the Virgo supercluster, $P_{\phi\rightarrow\gamma}$ can be large as long as n_e also decreases proportionately. Hence this phenomenon explains the alignment seen in this sample over very large angles.

It is clearly very important to further test the proposal that the align-

ment effect is due to pseudoscalar-photon mixing. Jain et al. (2002) have computed all the Stokes parameters of the electromagnetic wave in the presence of such a pseudoscalar particle. They find that the spectral dependence of the linear polarization, the circular polarization and the orientation angle of the linear polarization are all closely correlated with one another due to this mixing. This correlation can be studied by making further observations, which can establish or rule out this explanation.

In our discussion we have assumed an isotropic and homogeneous universe. We have not considered the possibility of a cosmological scale magnetic field or a Lorentz violating interaction (Nodland & Ralston 1997; Carroll, Field & Jackiw 1990), which might also explain these observations. A large scale dipole anisotropy is also observed in the radio polarizations from distant AGNs (Jain & Ralston 1999). This anisotropy was found to be independent of radial distances and might be explained in terms of some local effect. The axis of this dipole anisotropy is found to be pointing approximately opposite to the center of our local supercluster. Since this is a dipole anisotropy the effect on polarizations is large both in the direction and opposite to the axis. Hence the radio anisotropy displays an intriguing relationship to the large scale alignment seen in optical polarizations in the direction of the supercluster center. This might be a hint for a common origin of these two effects. The fundamental origin of the radio anisotropy is not known. Jain et al. (2002) pointed out that the existence of a light pseudoscalar can also explain this effect if the AGNs emit a large flux of pseudoscalars at radio frequencies. Although this explanation is disfavored due to the very large pseudoscalar flux required from the distant AGNs, it does explain the correlation between the radio dipole axis and the observed large scale alignment in optical polarizations.

6 Conclusions

In conclusion we have developed coordinate invariant statistical procedures in order to test for the large scale alignment of optical polarizations. We applied these tests to a data sample of QSOs compiled by Hutsemékers (1998) and Hutsemékers & Lamy (2001) and find that the polarizations show statistically significant alignment over very large distances. We find that the alignment is redshift dependent and is seen dominantly for the data sample with low polarizations ($p \leq 2\%$). We also find that the large redshift, $z \geq 1$, sample shows a very large scale alignment. Infact the polarizations contained in almost the entire data sample at $z \geq 1$ seem

to be correlated with one another. We find that galactic or supercluster extinction is unlikely to provide an explanation for these observations. We also argue that the existence of a hypothetical pseudoscalar particle might provide an explanation for the alignment effect.

Acknowledgements: We thank Gopal Krishna, Rajaram Nityananda, D. J. Saikia and Tarun Souradeep for useful discussions.

References

Ahluwalia D. V., Goldman T., 1993, Mod. Phys. Lett., A 28, 2623

Bietenholz M. F., 1986, AJ, 91, 1249

Brockway J. W., Carlson E. D., Raffelt G., 1996, Phys. Lett., B 383, 439 (astro-ph/9605197)

Carlson E. D., Garretson W. D., 1994, Phys. Lett., B 336, 431

Carroll S. M., Field G. B., Jackiw R., 1990, Phys. Rev., D 41, 1231

Csaki C., Kaloper N., Terning J., 2002, Phys. Rev. Lett., 88, 161302, (hep-ph/0111311)

Das P., Jain P., Mukherjee S., 2001, Int. Jour. of Mod. Phys., A 16, 4011 (hep-ph/0011279).

Grifols J. A., Masso E., Toldra R., 1996, Phys. Rev. Lett., 77, 2372

Harari D., Sikivie P., 1992, Phys. Lett., B 289, 67

Hutsemékers D., 1998, A & A, 332, 410

Hutsemékers D., Lamy H., 2001, A & A, 367, 381

Jain P., Panda S., Sarala S., 2002, Phys. Rev., D 66, 085007 (hep-ph/0206046)

Jain P., Ralston J. P., 1999, Mod. Phys. Lett., A 14, 417

Maiani L., Petronzio R., Zavattini E., 1986, Phys. Lett., B 175, 359

Mann R. B., Moffat J. W., 1981, Can. J. Phys., 59, 1730

Nodland B., Ralston J. P., 1997, Phys. Rev. Lett., 78, 3043

Peccei R. D., Quinn H., 1977, Phys. Rev., D 16, 1791

Raffelt G., 1999, Ann. Rev. Nucl. Part. Sci., 49, 163 (hep-ph/9903472)

Ralston J. P., 1995, Phys. Rev., D 51, 2018

Rosenberg L. J., van Bibber K. A., 2000, Phys. Rep., 325, 1

Sachs M., 1982, General Relativity and Matter, Reidel,

Sikivie P., 1983, Phys. Rev. Lett., 51, 1415

Vallee J. P., 1990, AJ, 99, 459

Will C. M., 1989, Phys. Rev. Lett., 62, 369

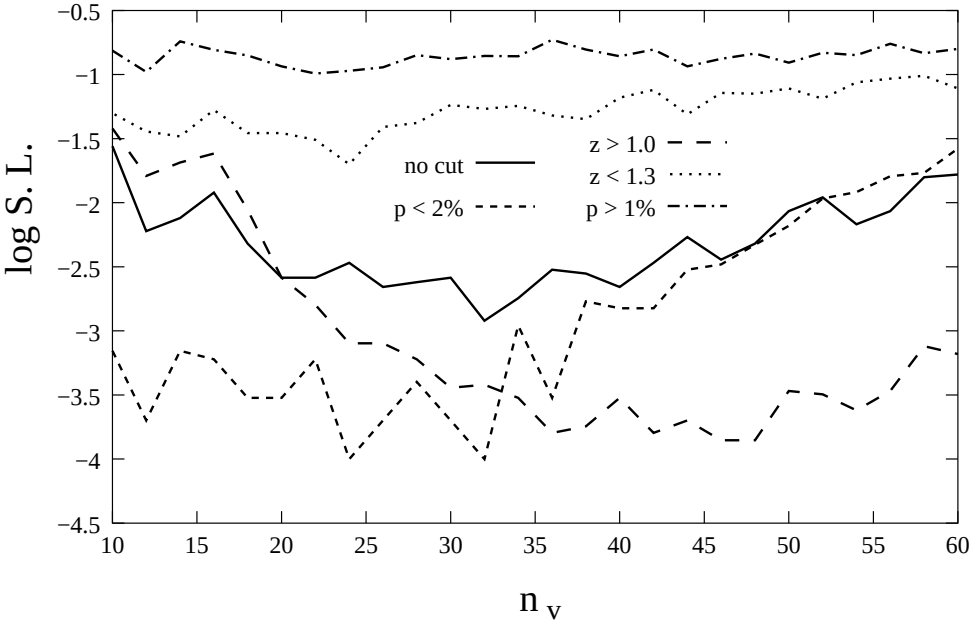

Figure 3: The logarithmic significance level, $\log(S.L.)$, as a function of the number of nearest neighbours n_v using the statistic S_D^p. The nearest neighbours are obtained by taking into account the radial distance of the source and hence this tests for redshift dependent alignment. The black curve corresponds to the entire data set. The short dashed, dash-dotted, long dashed and dotted curves correspond to the cuts $p \leq 2\%$, $p \geq 1\%$, $z \geq 1.0$ and $z \leq 1.3$ respectively.

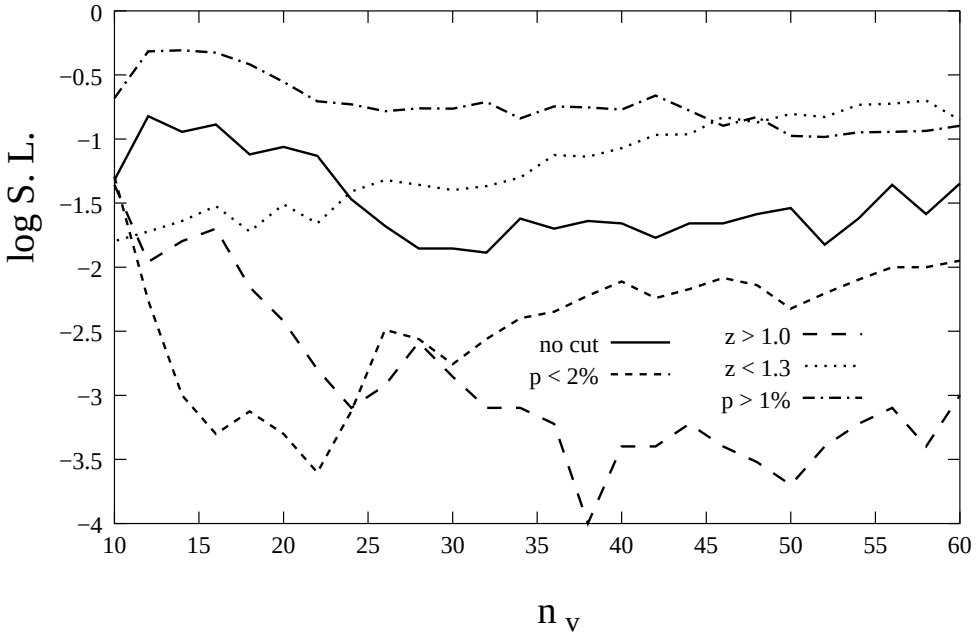

Figure 4: The logarithmic significance level, $\log(S.L.)$, as a function of the number of nearest neighbours n_v using the statistic S_D^p. The nearest neighbours are obtained without taking into account the radial distance of the source and hence this tests for redshift independent alignment. The black curve corresponds to the entire data set. The short dashed, dash-dotted, long dashed and dotted curves correspond to the cuts $p \leq 2\%$, $p \geq 1\%$, $z \geq 1.0$ and $z \leq 1.3$ respectively.

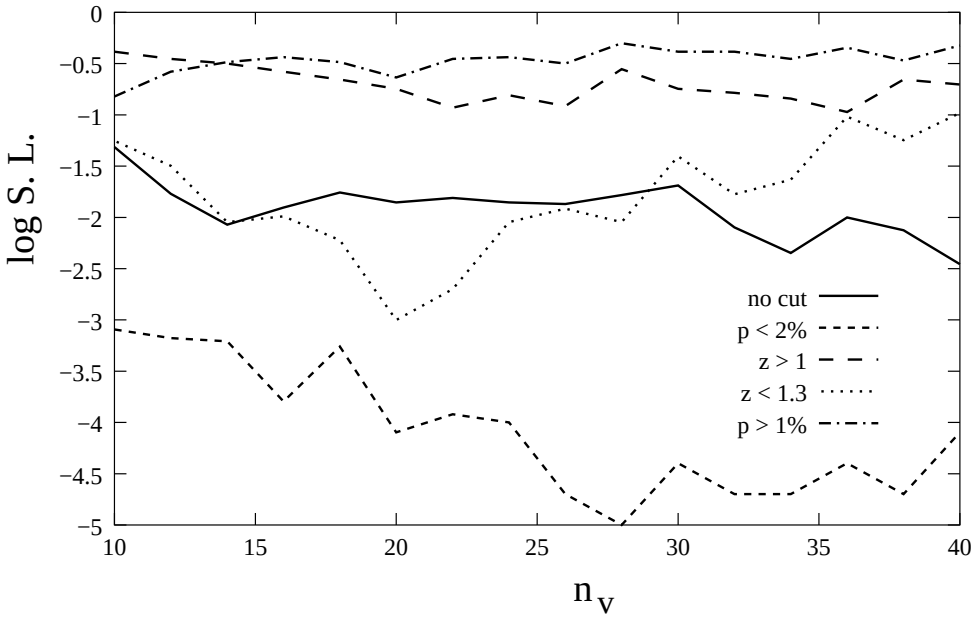

Figure 5: The logarithmic significance level, $\log(S.L.)$, as a function of the number of nearest neighbours n_v using the statistic Z_c^p. The nearest neighbours are obtained by taking into account the radial distance of the source and hence this tests for redshift dependent alignment. The black curve corresponds to the entire data set. The short dashed, dash-dotted, long dashed and dotted curves correspond to the cuts $p \leq 2\%$, $p \geq 1\%$, $z \geq 1.0$ and $z \leq 1.3$ respectively.

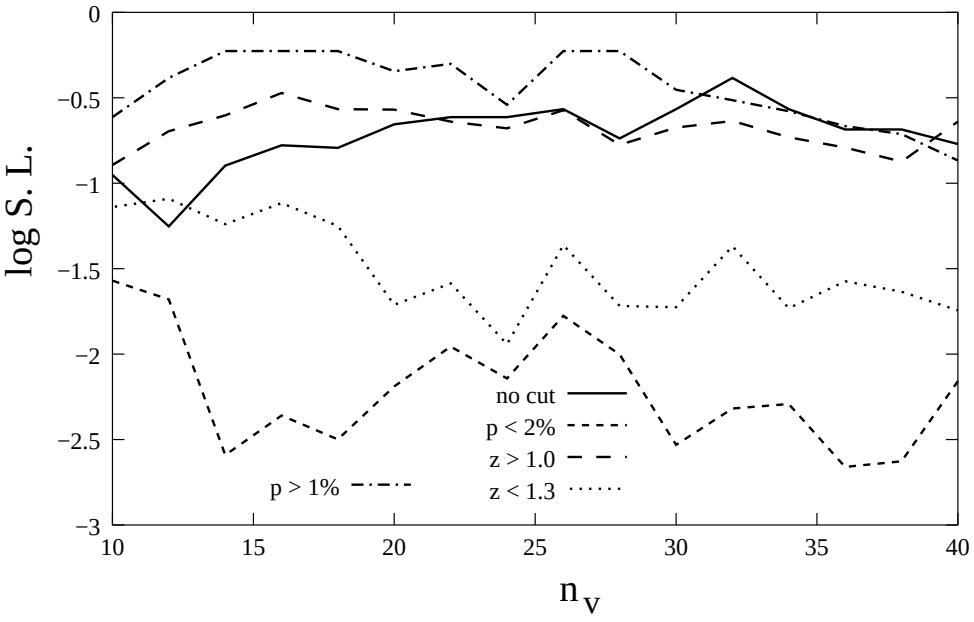

Figure 6: The logarithmic significance level, $\log(S.L.)$, as a function of the number of nearest neighbours n_v using the statistic Z_c^p. The nearest neighbours are obtained without taking into account the radial distance of the source and hence this tests for redshift independent alignment. The black curve corresponds to the entire data set. The short dashed, dash-dotted, long dashed and dotted curves correspond to the cuts $p \leq 2\%$, $p \geq 1\%$, $z \geq 1.0$ and $z \leq 1.3$ respectively.

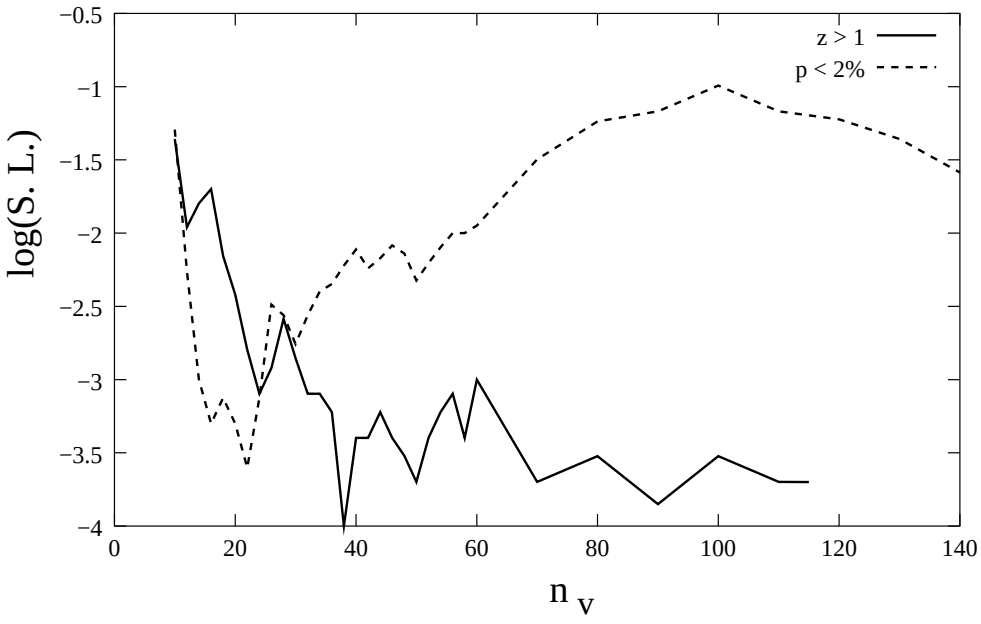

Figure 7: The logarithmic significance level, $\log(S.L.)$, as a function of the number of nearest neighbours n_v using the statistic S_D^p for the cuts $z \geq 1$ (solid curve) and $p \leq 2\%$ (dashed curve). The nearest neighbours are obtained without taking into account the radial distance of the source and hence this tests for redshift independent alignment. Results are shown for very large values of n_v and this tests for alignment over very large distances. The total number of points in the sets $z \geq 1$ and $p \leq 2\%$ are 115 and 146 respectively.

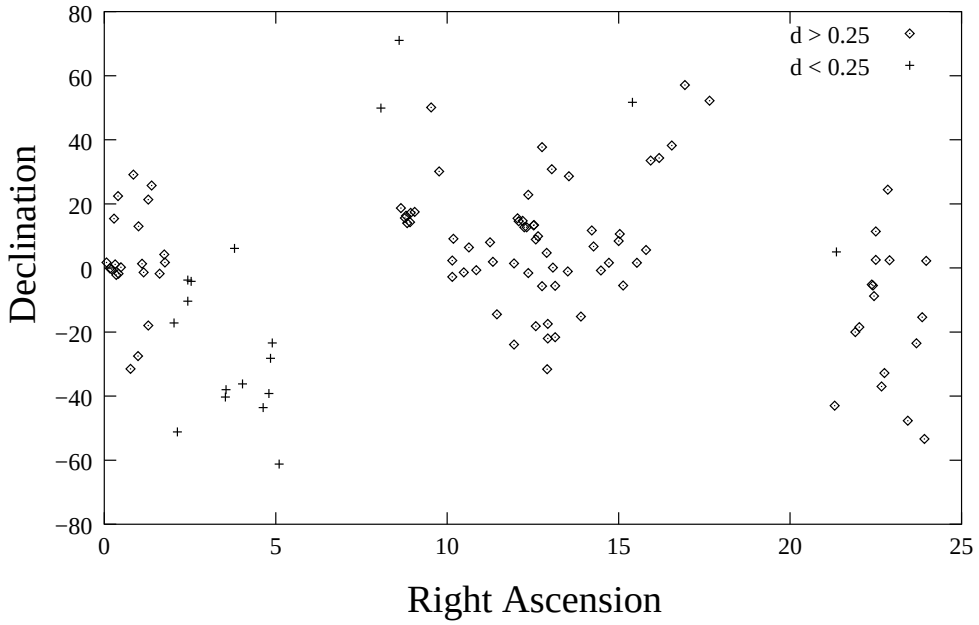

Figure 8: Scatter plot of the objects which show significant alignment $d_i > 0.25$ (dots) and those which do not show alignment $d_i < 0.25$ (pluses). Here d_i is a measure of the dispersion as defined in Eq. 14. The figure shows the data sample with the cut $z \geq 1$ with the number of nearest neighbours $n_v = 38$.